Advanced Oxygen Recovery via Series-Bosch Technology

Morgan B. Abney[1], J. Matthew Mansell[2], Bobby Atkins[3], Chris Evans[4], and Mononita Nur[5]
NASA George C. Marshall Space Flight Center, Huntsville, AL, 35802

and

Rockford D. Beassie[6]
The University of Texas at Arlington – Department of Mechanical & Aerospace Engineering, Arlington, TX, 76010

Advanced oxygen recovery life support for Martian transit and surface missions constitutes a variety of possible architectures. Over the last several years, NASA has pursued development of a two-step Bosch-based system called Series-Bosch (S-Bosch) to enable maximum recovery of oxygen from metabolic carbon dioxide. The first step of the process involves the Reverse Water-Gas Shift (RWGS) reaction. Two RWGS reactors, one developed at NASA and the other developed at Precision Combustion, Inc. have been assembled for the S-Bosch. The RWGS reactors were each tested to evaluate and compare general operational performance and fouling resistance. A down-select was completed to identify the reactor to be used in an integrated S-Bosch system. The second step in the S-Bosch process is carbon deposition. A carbon formation reactor (CFR) based on Martian regolith simulant as a catalyst was designed and tested for performance. Because the regolith will only be available once the crew arrives on the Martian surface, a second catalyst was evaluated for transit phases. Finally, integrated testing of an S-Bosch system was completed, leading to a technology readiness level (TRL) advancement of the S-Bosch system to TRL 4. The results of the RWGS down-select, CFR testing, and TRL evaluation are reported and discussed.

Nomenclature

BOP	=	Balance of Plant
CFR	=	Carbon Formation Reactor
CHXR	=	condensing heat exchanger
CO_2	=	Carbon Dioxide
CORTS	=	CO_2 Reduction Test Stand
ECLSS	=	Environmental Control & Life Support Systems
H_2	=	diatomic hydrogen
MSFC	=	Marshall Space Flight Center
MRS	=	Martian Regolith Simulant
MTR	=	Membrane Technology Research, Inc.
OGA	=	Oxygen Generation Assembly
RFMBR	=	Radial Flow Moving Bed Reactor
RWGSr	=	Reverse Water-Gas Shift reactor
S-Bosch	=	Series-Bosch

---

[1] Lead Aerospace Engineer, ECLSS Development Branch, Mail Stop: ES62, MSFC, AL 35812.

[2] Lead Test Engineer, ECLSS Development Branch, Bldg 4755, Room 115, MSFC, AL 35812.

[3] Mechanical Designer, Mechanical and Thermal Analysis Branch, Bldg 4877, MSFC, AL 35812.

[4] Simulation and Analysis, Marshall Space Flight Center, Al 35812.

[5] NASA Cooperative Student, ECLSS Development Branch, Bldg 4755, MSFC, AL 35812.

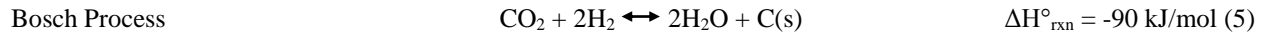[6] NASA Intern, ECLSS Development Branch, Marshall Space Flight Center, University of Texas at Arlington.
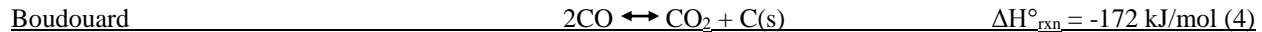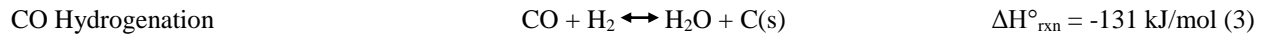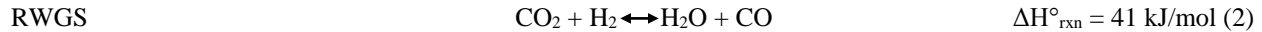
I. Introduction

OXYGEN recovery from metabolically-produced carbon dioxide (CO_2) is of critical importance for long-duration manned space missions beyond low Earth orbit. On the *International Space Station* (ISS), oxygen is provided to the crew through electrolysis of water in the Oxygen Generation Assembly (OGA). Prior to 2011, this water was entirely resupplied from Earth. A CO_2 Reduction Assembly based on the Sabatier reaction (1) was developed by Hamilton Sundstrand and delivered to ISS in 2010. The unit recovers oxygen by reducing metabolic CO_2 with diatomic hydrogen (H_2) to produce methane and product water. The water is cleaned by the Water Purification Assembly and recycled to the OGA for continued oxygen production. The methane product is vented overboard.

Sabatier Reaction $\qquad\qquad\qquad CO_2 + 4H_2 \leftrightarrow 2H_2O + CH_4 \qquad\qquad \Delta H^\circ_{rxn} = -165 \text{ kJ/mol (1)}$
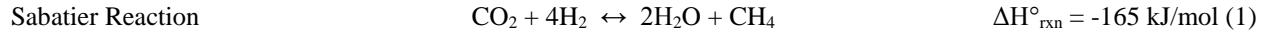
Ground testing of a Sabatier Development Unit with a design similar to the Hamilton Sundstrand hardware on board ISS, suggests that the expected system-level oxygen recovery of a life support architecture similar to that on ISS, but fully utilizing the Sabatier reactor, is just under 50% of the oxygen required to sustain the crew.[3] Thus, when the Sabatier unit is fully operational, this system results in a reduction in water resupply mass from Earth of over 530kg/year (>1180 lbs/year) for a crew size of four. While this savings is considerable, for missions beyond ISS such as Lunar or Martian surface missions, oxygen recovery of >90% has been identified as an enabling capability.[1] To achieve this goal, several post-processing technologies have been explored to generate H_2 from the Sabatier methane product stream and recycle it back to the Sabatier to enhance CO_2 conversion. These efforts have been reported previously.[2-6]

As an alternative to a Sabatier-based oxygen recovery architecture, the Bosch process has been proposed for future missions. This process provides 100% theoretical recovery of oxygen from metabolic CO_2 with the limited H_2 generated by the OGA. The Bosch process (5) has been discussed in detail previously[7-11] and involves a two-step mechanism to convert CO_2 and hydrogen to water and solid carbon. In the first step, CO_2 reacts with hydrogen in the Reverse Water-Gas Shift reaction (2) to form carbon monoxide (CO) and water. In the second step, the carbon monoxide is further reduced to solid, elemental carbon by either hydrogen (3), or by self-disproportionation in the Boudouard reaction (4).

RWGS $\qquad\qquad\qquad\qquad CO_2 + H_2 \leftrightarrow H_2O + CO \qquad\qquad\qquad \Delta H^\circ_{rxn} = 41 \text{ kJ/mol (2)}$

CO Hydrogenation $\qquad\qquad\qquad CO + H_2 \leftrightarrow H_2O + C(s) \qquad\qquad\qquad \Delta H^\circ_{rxn} = -131 \text{ kJ/mol (3)}$

Boudouard $\qquad\qquad\qquad\qquad 2CO \leftrightarrow CO_2 + C(s) \qquad\qquad\qquad \Delta H^\circ_{rxn} = -172 \text{ kJ/mol (4)}$

Bosch Process $\qquad\qquad\qquad CO_2 + 2H_2 \leftrightarrow 2H_2O + C(s) \qquad\qquad\qquad \Delta H^\circ_{rxn} = -90 \text{ kJ/mol (5)}$

Over the last several years, NASA has supported development of a Series-Bosch (S-Bosch) system as shown in Figure 1. The major components of the S-Bosch are a Reverse Water-Gas Shift reactor (RWGSr), carbon formation reactor (CFR), compressor, condensing heat exchanger (CHXR), and two separators. The
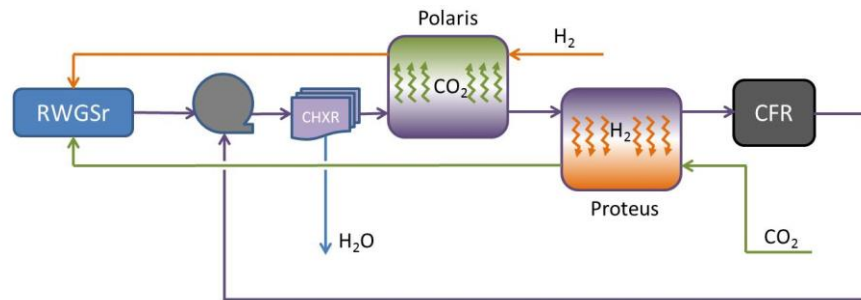

Figure 1. Series-Bosch Approach for Oxygen Recovery.

separators currently in use are based on two membrane materials developed by Membrane Technology Research, Inc. (MTR). The Polaris and Proteus membrane separators separate CO_2 and hydrogen, respectively, from the bulk gas within the CFR loop. The permeate gases are mixed with fresh H_2 and CO_2, and then recycled back to the RWGSr. The retentate gas stream, which continues to the CFR, contains a high concentration of CO. By effecting these separations, the single-pass conversion of both reactors is greatly enhanced. The CFR converts CO to solid carbon by (3) and (4). The CFR effluent mixes with the RWGSr effluent, and then passes through the CHXR, where water is

condensed out of the stream, before returning to the membrane separators. Because the permeation rates through the membranes increase with the partial pressure differentials across the membrane (retentate pressure minus permeate pressure), and the selectivities of the membranes are expected to be relatively high, the system is operated with the permeate side at a lower total pressure than the retentate side of the system.

In 2014, progress of S-Bosch development was reported.[6] At that time, the system contained only the RWGSr, the Polaris membrane separator, and the Proteus membrane separator, along with the balance of plant (BOP) components required to control and monitor the partially completed system. Testing to gather data on thermal behavior of the RWGSr had been conducted and was reported, but no other testing had been completed. Since that time, continued development at the NASA Marshall Space Flight Center (MSFC) has involved performance mapping of the RWGSr, performance mapping of both membrane separators, design and assembly of a "batch" CFR, and initial testing of this CFR with both a proposed Martian surface mission catalyst and a Martian transit mission catalyst. This paper includes discussion of the results of recent testing, updates on the status of the project, an operational evaluation of the S-Bosch approach, and a discussion of the advantages of the S-Bosch architecture.

II.   Materials and Methods

Four tests were conducted to evaluate the performance of the RWGSr, Proteus Membrane, Polaris Membrane, and CFR sub-systems of the S-Bosch in stand-alone configurations. The materials and methods for each test are provided below.

A. CO₂ Reduction Test Stand (CORTS)

The performance evaluations of these four sub-systems were conducted on the CO_2 Reduction Test Stand (CORTS) at the MSFC Environmental Control and Life Support Systems (ECLSS) development facility. The CORTS provides the capability to test integrated systems or evaluate the performance of each sub-system individually by controlling system parameters (e.g. flow rates, temperatures, pressures, etc) and providing data acquisition from all system controls and sensors. The CORTS includes an Agilent 3000 micro-gas chromatograph for dry gas analysis and a General Eastern Optica Series DewPoint Analyzer to determine the water vapor content of gas streams. The CORTS test stand is controlled using internally developed Labview software. Data is collected and stored using an internal MSFC software called PACRATS.

Ultra-high purity gas was used for all testing on the CORTS. Hydrogen, nitrogen, carbon dioxide, argon, and helium were supplied by Sexton Gas and Airgas. Carbon monoxide was purchased from Matheson Tri-Gas.

B. RWGSr Performance Testing Methods

The RWGSr, discussed in detail previously and shown in Figure 2, was tested at a range of operating points to evaluate the anticipated performance under various metabolic and off-nominal conditions. Based on thermal testing of the reactor, it was determined that a regenerative heat exchanger is critical to RWGSr heating. Thus, a pre-heater was used in all testing to mimic regenerative heating of the inlet gas to the RWGSr. The pre-heater was set to 400° C. A full factorial test was conducted with the range of variables shown in Table 1. The heater setpoints were chosen based on the thermodynamic favorability of the RWGS reaction at these temperatures over the Sabatier reaction. The CO_2 feed rates represent the average production of a crew of four (1.41 SLPM), and double that rate (2.82 SLPM) to account for expected recycled gas rate. The $H_2:CO_2$ ratios were chosen based on stoichiometry (1:1), anticipated actual feed to the RWGSr (2:1), and a stress case (3:1). RWGSr test pressures were selected based on expected habitat pressure. Martian surface mission concepts reported over the past several years typically reference habitat pressures of 70.3 kPa (10.2 psia) or 57.2 kPa (8.3 psia).[12] RWGSr inlet pressures were chosen to correspond to system operation with maximum pressures below 70.3 kPa.

Table 1. RWGSr Performance Testing Variables.

Parameter	Values
RWGSr Heater Set Points	600°C, 650°C, 700°C
CO2 Feed Rates	1.41 SLPM, 2.82 SLPM
H2:CO2 Ratios	1:1, 2:1, 3:1
RWGSr Inlet Pressure	20.7 kPa (3 psia), 34.5 kPa (5 psia), 55.1 kPa (8 psia)

Figure 2. Reverse Water-Gas Shift Reactor with band heaters and integrated thermocouples.

C. Membrane Performance Testing Methods

The two separation membranes were individually evaluated for performance. The membranes are constructed with two sides: the process (retentate) side and the sweep (permeate) side. The composition, pressure, and flow rate of gas on either side of the membrane is controlled. Gas flow through the sweep side of the membrane facilitates removal of permeate compounds, thereby maximizing the concentration gradients across the membrane and enhancing permeation. For any given compound, the permeation rate through a membrane increases with increased pressure ratio (process pressure/sweep pressure). Selectivity of the membranes is highest at the optimum membrane temperature.

Because we plan to operate the S-Bosch below the surrounding air pressure of the habitat, the maximum pressure of either side of each membrane must not exceed the cabin pressure. Thus, the process (high pressure) side of the membranes was varied. A constant nominal differential pressure of 34.5 kPa (5psid) was targeted for testing of both membranes. Carbon dioxide was used as the sweep gas for the Proteus (to separate H_2), and H_2 was used as the sweep gas for the Polaris (to separate CO_2). The optimum operating temperature for the Polaris membrane, per MTR specifications, is less than 20°C. We did not attempt to cool

Table 2. Polaris and Proteus Membrane Testing Variables.

Parameter	Values
Membrane Process Side Pressure	55.1 kPa (8 psia), 68.9 kPa (10 psia), 89.6 kPa (13 psia)
Membrane Temperature	Ambient, 111°C (Proteus only), 130°C (Proteus only)
Sweep Gas "Low Flow" Rate	0.7 SLPM (Proteus), or 1.41 SLPM (Polaris)
Sweep Gas "High Flow" Rate	1.41 SLPM (Proteus), or 2.82 SLPM (Polaris)
Process Feed Composition	
H_2	27-63 mol%
CO_2	16-41 mol%
CO	15-24 mol%
CH_4	0-0.26 mol%

the membrane, but designed the test to maintain the Polaris membrane near room temperature. The Proteus membrane was specified to operate most efficiently at 125-135°C. For the Proteus, the initial test matrix included ambient temperature (to mimic operation in case of a heater power failure) and 130°C operation. However, a problem with the heater controller resulted in test data collection at 111°C. The test was repeated at 130°C after repairing the heater controller. Thus, the Proteus was operated at 130°C, 111°C, and ambient temperature (~20°C). Finally, all gas fed to the process sides of the membranes was generated by passing mixtures of CO_2, H_2, and N_2 first through the RWGSr and then to the membranes. The composition of the gas fed to the process side of the membrane was varied by varying the feed to the RWGSr. All membrane testing variables are provided in Table 2. Data reduction was completed using Microsoft Office Excel and Minitab 16.

D. CFR Reactor and Performance Testing Methods

The considerations for a CFR based on Martian regolith simulant (MRS) catalyst were discussed previously.[7] With these considerations, a design for a 1st generation CFR (hereafter referred to simply as "the CFR") was completed and then fabricated. The reactor is made up of four concentric cylinders as shown in Figure 3. A cartridge heater runs along the central axis of the reactor.
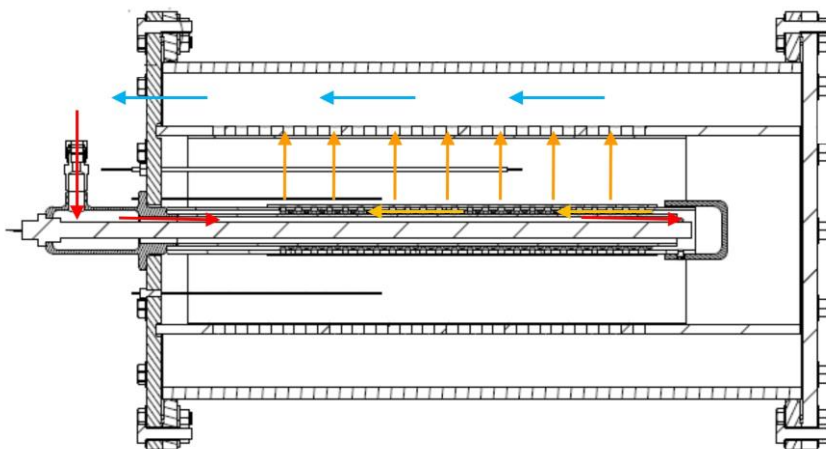

Figure 3. CFR Catalyst Bed Flow Diagram. *Gas enters the reactor and flows down the annulus between the heater and the core cylinder (red arrows). The gas exits the core cylinder and flows between the core and second cylinders (yellow arrows). The gas enters the catalyst bed through perforations in the second cylinder, flows through the bed, and exits through perforations in the third cylinder (orange arrows). After exiting the catalyst bed, the gas enters the void between the third and fourth cylinders and exits the reactor (blue arrows).*

4

Feed gas enters at a header at the top of the reactor. The gas flows along the length of the heater through a narrow annulus between the heater and the first concentric cylinder. The majority of the heat transfer to the gas takes place in this section of the reactor. The hot gas exits the annulus into a void between the first and second cylinders. The second cylinder is perforated along most of its length and is covered in copper mesh to contain the MRS catalyst. Gas passes radially outward through the perforations in the second cylinder and into the catalyst bed, which is formed by the space between the second and third concentric cylinders. The third cylinder, also perforated and covered in copper mesh, is located on the outside of the catalyst bed. Gas continues to flow radially through the bed, and ultimately exits through the perforations in the third cylinder. The fourth cylinder is the outer housing of the reactor. Gas flows through the catalyst bed, out of the third cylinder into the void between the third and fourth cylinders. The reactor outlet is located at the top of the reactor, positioned radially between the outer surface of the third cylinder and the inner surface of the reactor wall (the fourth cylinder). This design provides a high temperature at the inlet to the catalyst bed (i.e., the outer surface of the second cylinder). This high temperature is kinetically favorable for conversion of CO. A negative radial temperature gradient through the reactor provides the thermodynamically favorable conditions (i.e. lower temperatures at the catalyst bed outlet) to maximize net conversion to solid carbon.

Three reactor designs were completed: a batch reactor design (the first generation design described above), a semi-batch reactor design, and a continuous reactor design. The batch reactor provides a comparatively low-cost option to test the radial-flow concept and the MRS catalyst performance. This design does not allow addition or removal of catalyst during operation. The semi-batch reactor design enables the removal (but not addition) of solid material from the catalyst bed without shutting down the reactor heaters or cooling the bed. Finally, the continuous reactor design enables both the removal of solid material from the bed and the addition of fresh catalyst to the bed during operation.

Due to the limited availability of funding, the batch reactor, shown disassembled in Figure 4, was fabricated. The reactor was tested with two catalysts. The first catalyst, Martian Regolith Simulant (MRS), is envisioned as an option for long-duration operation on the Martian surface where the regolith material might be used as an *in situ* resource. The second catalyst, iron beads, is the proposed catalyst to be used for transit missions and as a risk mitigation approach for the MRS. The CFR was first packed and tested with MRS purchased from Orbital Technologies and sieved to include particle sizes 355-1000μm. The packed reactor was installed into a CFR sub-assembly and integrated into CORTS for testing. At the completion of the MRS test, the CFR was packed with Amasteel S-660 steel beads purchased from Ervin Industries.

Initial testing of the CFR with each catalyst was conducted to evaluate the actual performance compared to predicted performance based on sub-scale catalyst testing and based on thermal models prepared during the reactor design. All testing of the CFR was conducted at an inlet pressure of 93.1 kPa (13.5 psia). Gas

Figure 4. Fabricated Batch CFR. *CFR shown in three parts: the outer (fourth) cylinder (on left), the reactor top cap connected to the perforated third cylinder covered with copper mesh and containing the second cylinder end cap (center), and the reactor bottom cap (right).*

Table 3. CFR Performance Testing Variables: MRS Catalyst.

Parameter	Values
CFR Heater Temperatures	700°C, 750°C
CFR Pre-Heater Temperatures	0°C, 150°C, 400°C
CO Feed Rates	0.195-1.000 SLPM
H_2 Feed Rates	0.195-1.000 SLPM

Table 4. CFR Performance Testing Variables: Steel Bead Catalyst.

Parameter	Values
CFR Heater Temperature	750°C
CFR Pre-Heater Temperatures	400°C
CO Feed Rates	0.195-2.000 SLPM
H_2 Feed Rates	0.195-2.080 SLPM

inlet composition, reactor heater temperature, and reactor pre-heater temperature were varied during testing of both the MRS catalyst as shown in Table 3, and the steel bead catalyst as shown in Table 4.

III. Results and Discussion

Four tests were undertaken to evaluate S-Bosch sub-assemblies including RWGSr Performance Testing, Proteus Separation Membrane Performance Testing, Polaris Separation Membrane Performance Testing, and CFR Performance Testing using MRS and iron beads as catalyst. The results of these tests and a discussion of their relevance are provided below. Additionally, a discussion of the S-Bosch system architecture is provided.

A. RWGSr Performance Testing Results and Discussion

A full factorial test was conducted to map the performance of the RWGSr by varying reactor temperature, pressure, CO_2 feed rate, and $H_2:CO_2$ feed ratio. Test requirements specified CO_2 feed rates of either 1.41 SLPM or 2.82 SLPM and a constant N_2 feed rate of 0.25 SLPM for mass balance calculations. After the tests were completed, it was determined that an error in the software had resulted in incorrect gas metering of the CO_2 and N_2 gases. Additionally, it was determined that the software controls assumed the mass flow controllers had been calibrated with a standard temperature of 0°C when the controllers had actually been calibrated at 25°C. The data from the test was adjusted accordingly and the actual gas flow rates to the RWGS reactor are shown in Table 5.

Table 5. Targeted versus Actual Set Point Values During RWGSr Performance Testing.

Variable	Targeted Set Point	Actual Set Point
N_2 Feed Rate (SLPM)	0.25	0.19
CO_2 Feed Rate (SLPM)	1.41	1.55
	2.82	3.10
$H_2:CO_2$ Molar Ratio	1	0.81
	2	1.66
	3	2.51

Empirical data collected during testing were compared with both thermodynamic equilibrium calculations and predicted performance based on COMSOL Multiphysics modeling conducted prior to the fabrication of the RWGS reactor.[10] Thermodynamic equilibrium represents the best theoretical performance achievable at a given temperature. The COMSOL predictive model goes one step further and incorporates limitations based on thermal variations, kinetic limitations, and geometric constraints. Figure 5 provides a visual comparison of the empirical data to thermodynamic equilibrium and the COMSOL predictions. The y-axis provides the CO_2 conversion via the RWGS reaction in mole %. The x-axis denotes the Data Point as described in Table 6.
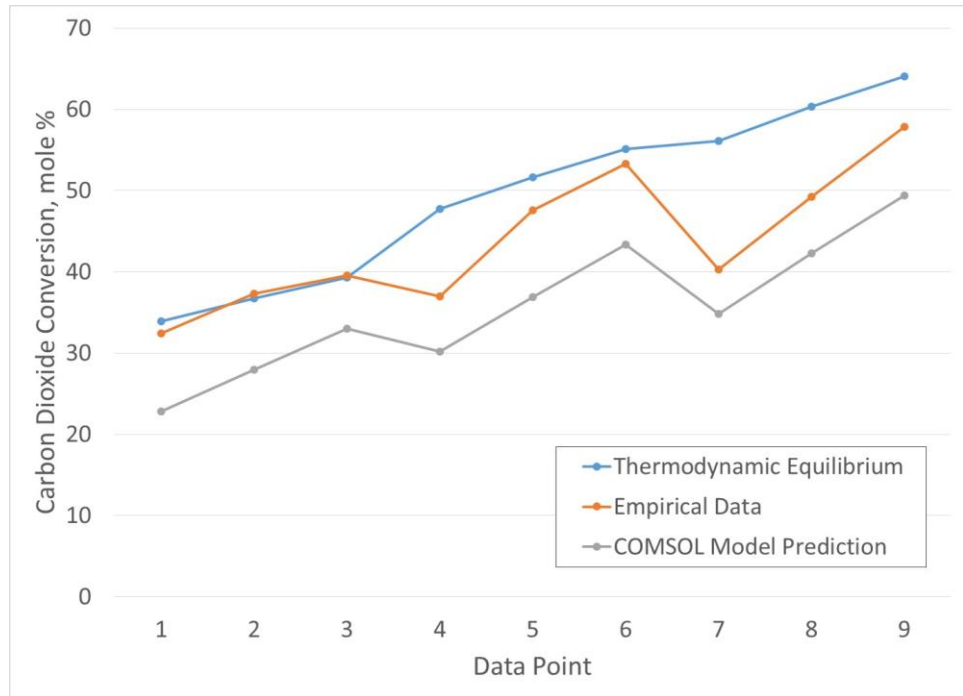

Figure 5. Comparison of Empirical RWGS Data with Thermodynamic Equilibrium and COMSOL Predictive Modeling. *Representative data collected at a reactor pressure of 8.0 psia and a CO_2 feed rate of 1.55 SLPM.*

International Conference on Environmental Systems

For the lowest molar ratio, and correspondingly lowest flow rate (Data Points 1-3), thermodynamic equilibrium was achieved in the reactor. None of the other data points were observed to achieve thermodynamic equilibrium. At the highest temperature of 700°C, equilibrium was approached (Data Points 6 and 9). As the temperature decreased (Data Points 4, 5, 7, and 8) the observed performance fell further from equilibrium. This is believed to be due to a combination of kinetic limitations at the lower temperatures and mass transport limitations at the higher flow rates. Interestingly, the trend of the COMSOL prediction closely matched the observed performance. However, COMSOL predicted approximately 10% lower molar conversion at all data points. This is believed to be do to variations in the calculated kinetic parameters from sub-scale testing and the actual kinetic parameters of the catalyst. Future analysis will identify the apparent kinetic parameters to improve the accuracy of the model and to more accurately predict potential off-nominal cases.

Pressure, while thermodynamically irrelevant in the case of the RWGS reaction under ideal conditions due to Le Chatelier's principle, will affect the overall residence time of the gas in the reactor, thereby potentially affecting conversions. This was observed to a limited degree in RWGSr testing as shown in Figure 6. The increase in pressure results in slightly higher CO_2 conversion to CO. Three pressures were targeted for RWGSr performance testing. However, the vacuum pump was unable to achieve the lowest pressure of 20.7 kPa (3psia) at the 1.66 and 2.51 H_2:CO_2 ratio feed rates. For data collected at a CO_2 feed rate of 3.10 SLPM, the pump was capable of maintaining 34.5kPa (5 psia) for only the 0.81 H_2:CO_2 ratio and was unable to achieve pressures below 55.1 kPa (8 psia) for the higher ratios. Regardless, a general trend in the data was observed based on the testing and is sufficient to extrapolate predictions of the performance at the higher flow rates.

Table 6. Explanation of Data Points for RWGS Stand-Alone Testing.

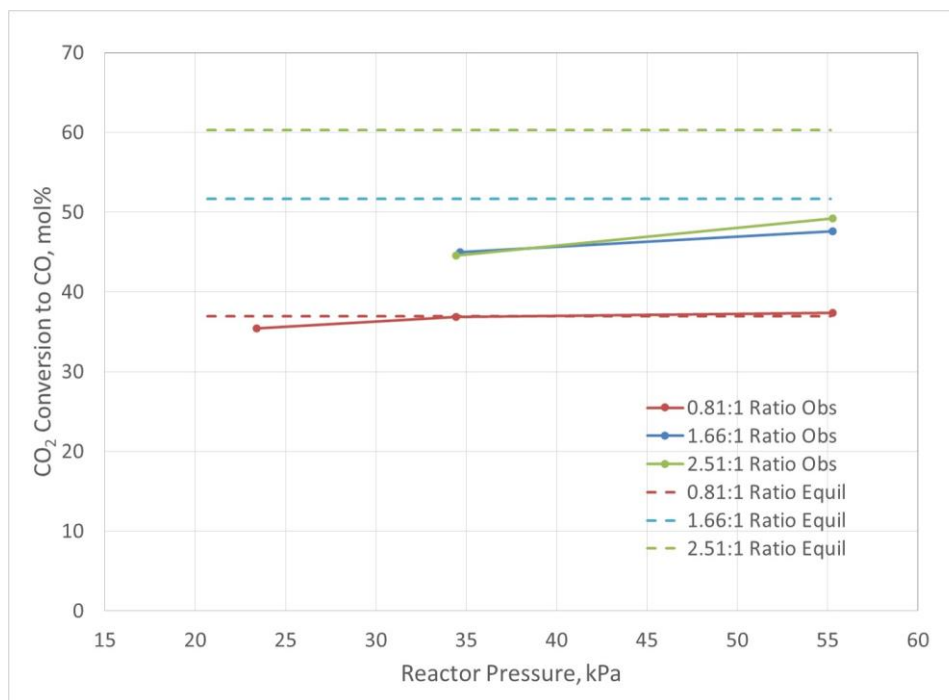| Test Point	Ratio of H_2:CO_2	Temperature (°C)
1	0.81	600
2	0.81	650
3	0.81	700
4	1.66	600
5	1.66	650
6	1.66	700
7	2.51	600
8	2.51	650
9	2.51	700

Figure 6. Pressure dependence on CO₂ conversion to CO in the RWGS reactor. *Representative data collected at a reactor temperature of 650℃ and a CO₂ feed rate of 1.55 SLPM. Solid lines not intended to suggest a fit of the data, rather used to draw the eye to the discrete data points observed during testing. Dashed lines indicate the equilibrium conversions for each H_2:CO_2 ratio.*

B. Proteus Separation Membrane Performance Testing Results and Discussion

A range of gas compositions was fed to the process side (high pressure) of the Proteus while feeding either a low flow (0.64 SLPM) or high flow (1.28 SLPM) pure CO_2 on the sweep side (low pressure). These values of CO_2 are slightly lower than originally intended due to a similar mass flow controller software issue as that observed in RWGSr Performance Testing. The data from testing was analyzed using Minitab 16 to evaluate main effects and factor

International Conference on Environmental Systems

interactions. Factors considered included the pressure ratio (process pressure/sweep pressure) across the membrane, the process stream inlet absolute pressure, the membrane temperature, the sweep flow rate, the H_2 feed rate in the process stream, and the total feed rate of the process stream. Responses included total hydrogen permeation, relative hydrogen permeation, and total percent mass permeation. The total % hydrogen permeation was calculated by analyzing the total hydrogen in the sweep stream at the outlet of the membrane and comparing to the total hydrogen fed to the process side. Relative hydrogen permeation was calculated by Eq 6.

$$relative H_2 Permeation(\%) = \frac{Total H_2 Permeated\,(g/\min)*100}{Total Gas Permeated\,(g/\min)} \qquad (6)$$

Total percent mass permeation is defined by the fraction of the total mass in the process side feed stream that exits the separator in the sweep stream. This value was calculated by Eq 7.

$$Total\%MassPermeation = \frac{(processInletMass(g/\min) - processOutletMass(g/\min))*100}{processInletMass(g/\min)} \qquad (7)$$

Table 7 provides a summary of the main effects observed in the Minitab 16 data reduction. A flat line indicates no influence of the factor on the response was observed. An arrow pointing upward indicates that an increase in the factor increased the response. Likewise, an arrow pointing downward indicates that an increase in the factor decreased the response. Note that for all data, a p-value <0.05 indicates a significant influence. Unexpectedly, neither the pressure ratio nor the sweep rate had a significant effect on the responses. A full main effects plot of total mass permeation versus pressure ratio is shown in Figure 7 as an example. This is contrary to the known operation of membrane systems where pressure and concentration gradients play critical roles in permeation. It is probable that the pressure ratio across the membrane was insufficient to have a significant influence on the permeation of the gases. Similarly, it is probable that the sweep gas flows were either too low to significantly influence permeation or were too similar for the test to have shown a difference based on the flow rates chosen. Process pressure also showed no influence

Table 7. Main Effects on Relative H₂ Permeation, % H₂ Permeation, and Total % Mass Permeation observed during testing of Proteus Separation membrane.

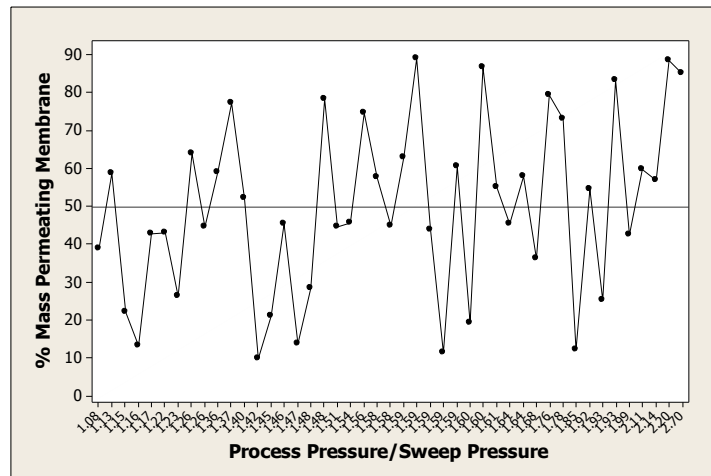| Factor	Relative H$_2$ Permeation, %	% H$_2$ Permeation, %	Total % Mass Permeation, %
Pressure Differential	---	---	---
Sweep Rate	---	---	---
Process Pressure	---	---	---
Membrane Temperature	↑	---	↑
Process H$_2$ Feed Rate	↑	↓	↓
Total Process Feed Rate	↑	↓	↓

Figure 7. Main effects plot showing the percentage of mass permeating the Proteus membrane from the process to the sweep side as a function of pressure ratio.

on the listed main effects. In general, this is as expected, since it is the pressure ratio that is understood to affect permeation. In a simplistic model, lower absolute pressures will result in higher mean molecular velocities through the membrane, but proportionally lower densities, leading to the same flux regardless of total pressure.

The percentage of available hydrogen permeating across the membrane was shown to decrease as the total flow rate of hydrogen in the process gas stream increased. This suggests that the permeation becomes increasingly diffusion

8

limited as the total mass flow increases and that additional hydrogen could be separated at the higher flow rates if the membrane had a higher surface area.

The percent hydrogen permeation also showed very interesting results. As can be seen in the main effects plot in Figure 8, as well as the permeation percentages of other species shown in Figure 9, at ambient temperature, all species equilibrated quickly between the process and sweep sides of the membrane. We believe the membrane porosity is much greater at ambient temperature, allowing all gases to permeate. As the temperature increased to 111°C, permeation of all species decreased significantly, this could be due to the membrane expanding and producing a better seal between the process and sweep sides, or due to the pore size of the membrane decreasing with the increased temperature and limiting the permeation, or a combination of both. When the temperature reached the

Figure 8. Main effects plot of H$_2$ permeation as a function of membrane temperature and process feed in the Proteus Membrane.

optimum temperature of 130°C the hydrogen permeation again increased. By looking at the percent permeations of the other gas constituents, shown in Figure 9, it can be seen that the permeation rates of all other species either continued to decrease or increased by much less than hydrogen. The fact that only hydrogen permeation increased at the 130°C setpoint confirms the relative selectivity of the membrane. Behavior below 130°C supports MTR's specification of that temperature as the optimum. The failure of the membrane to obstruct the flux of any compound at ambient temperature is an important result to be considered in analyzing subsystem-level failure risks.

Finally, the total percent mass permeation across the Proteus membrane was affected by the membrane temperature
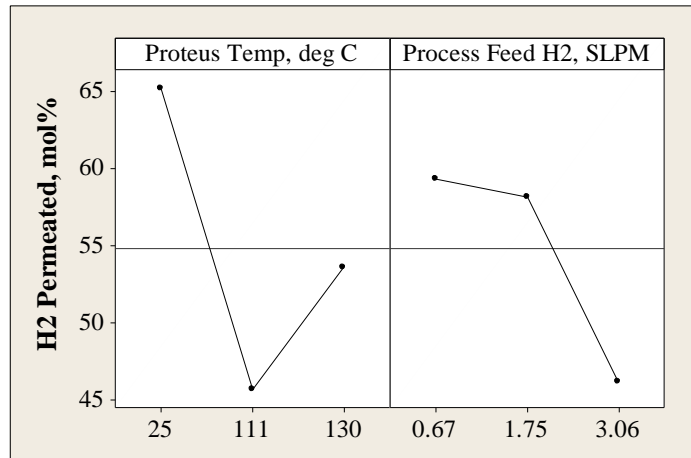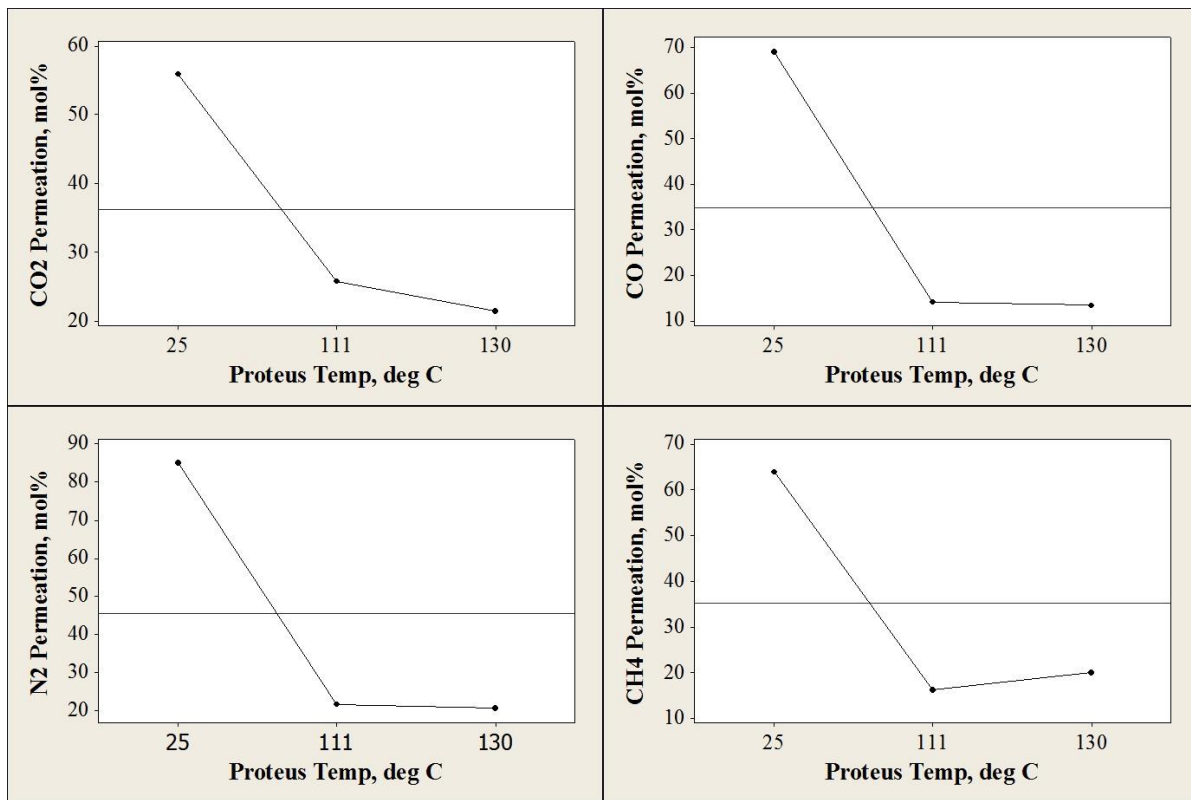

Figure 9. Percent permeation of CO$_2$ (upper left), CO (upper right), nitrogen (lower left), and methane (lower right) as a function of membrane temperature.

International Conference on Environmental Systems

and the total hydrogen/process feed rate. When the membrane temperature increased, total mass permeation increased. Because non-hydrogen components were observed to decrease with increasing temperature, it follows that this increase is due entirely to increased H_2 permeation. As total hydrogen/process feed rate increased, the total mass permeating the membrane decreased. Again, this can be explained by the reduction in CO, methane, CO_2, and nitrogen permeation.

C. Polaris Separation Membrane Performance Testing Results and Discussion

Similar to the Proteus membrane, the Polaris membrane is designed to selectively permeate gas at a high pressure differential (>345 kPa, >50 psid). However, while the Proteus is selective for hydrogen, the Polaris is selective for CO_2 and at ambient or colder temperatures. Like the Proteus, the Polaris cannot be operated at high pressure differentials in a life support system so a lower pressure differential (~34.5kPa, ~5psid) was targeted. This was combined with a sweep stream containing pure hydrogen to pull CO_2 across the membrane. A range of gas compositions was fed to the process side of the Polaris (identical to those fed to the Proteus) while feeding either a low flow (1.30 SLPM) or high flow (2.60 SLPM) pure hydrogen on the sweep side. These values of hydrogen are slightly lower than originally intended due to a similar mass flow controller software issue as that observed in RWGSr Performance Testing and the Proteus Separation membrane performance testing. The data from testing was analyzed with Minitab 16 to evaluate Main Effects. Factors considered included the pressure ratio across the membrane, the process pressure, the membrane temperature, the H_2 sweep flow rate, the CO_2 feed rate in the process stream, and the total feed rate of the process stream. Responses included total CO_2 permeation, Relative CO_2 Permeation, and total percent mass permeation. The total % CO_2 permeation was calculated by analyzing the total CO_2 in the sweep stream at the outlet of the membrane and comparing to the total CO_2 fed to the process side. Relative CO_2 Permeation was calculated by Eq 8.

$$relative CO_2 Permeation (\%) = \frac{Total CO_2 Permeated\ (g/\min)*100}{Total Gas Permeated\ (g/\min)} \tag{8}$$

Total percent mass permeation is defined by the total mass initially in the process side of the membrane that permeates the membrane to the sweep side of the membrane. This value was calculated by Eq 7 above.

Several observations were made during testing of the Polaris membrane. First, it proved impossible to maintain the targeted 34.5 kPa (5psid) pressure differential across the membrane. This led to the hypothesis that there was a hole in the membrane and that the two sides of the membrane were simply equilibrating. It was determined from the GC results that all the components were permeating the membrane in similar quantities, as seen in Figure 10. As can be seen, more than 75% of all of the gases
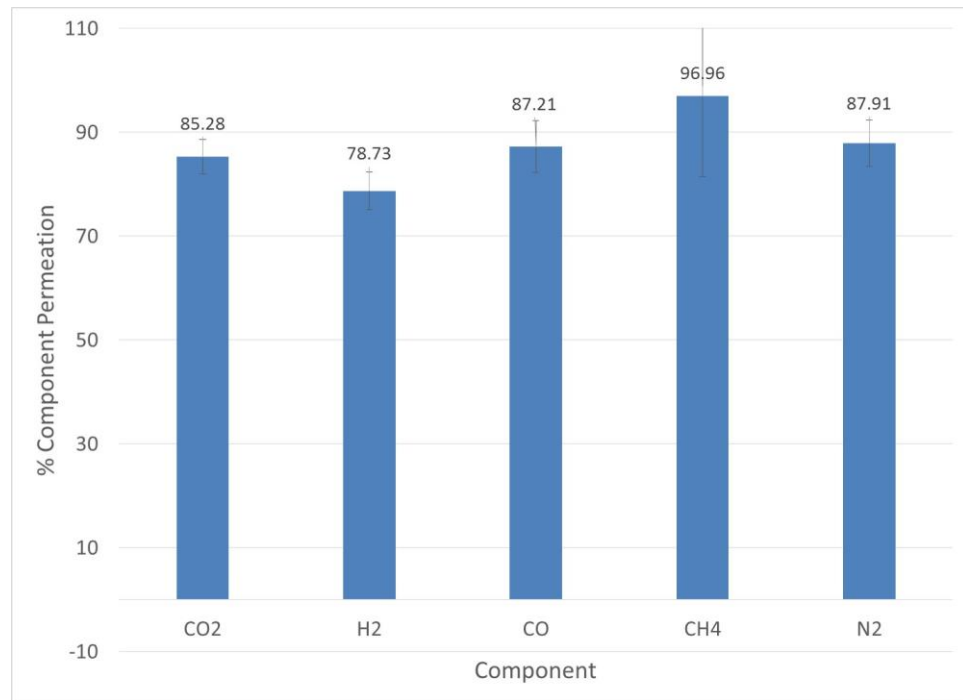
Figure 10. Average gas permeation across the Polaris membrane. *Data was collected at ambient temperature and various pressures and feed rates. Error bars represent standard deviation.*

permeated the membrane in a single pass. Additionally, the error bars, representing standard deviation, show how little variation there was regardless of pressure differential, flow rates, inlet gas composition, etc.

Based on this data, the hardware was disassembled at the end of the test to evaluate the internal membrane material. Two observations were made during this effort. First, as shown in Figure 11, the top sheet of membrane material was observed to have a significant tear. It is not clear if this tear occurred when the casing was opened or if the tear was present during testing and contributed to the unexpectedly low performance. Second, when the torn membrane sheet was removed and subsequent leak checks were performed, it was determined that the process and sweep sides of all the membrane sheets were not well sealed from one another, thus allowing a high leak rate between the two sides. Thus, regardless of the origin of the tear, a significant leak was measureable.
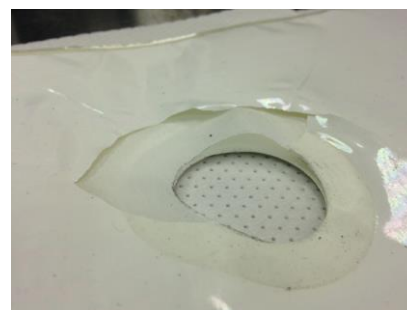

Figure 11. Tear observed in the special-design Polaris membrane sheet.

While leaking of the membrane caused considerable challenges to the reported testing, it is important to note that the membrane design and packaging was specific to test requirements for S-Bosch technology development, and not MTR's standard design. During initial discussions with MTR, a commercial-off-the-shelf (COTS) Polaris membrane was offered with their standard packaging (spiral-wound membrane sheets in a cylindrical housing) that has years of demonstrated reliability and performance. However, the COTS option did not provide the flexibility to modify surface area (by removing or adding membrane sheets). For this reason, a unique, one-of-a-kind approach to the Polaris membrane and housing was attempted for S-Bosch development purposes. The intention was to use the unique modifiable design to correctly size the required membrane surface area and have MTR manufacturer a COTS unit with the optimum surface area for the final S-Bosch system. Thus, despite the fact that this membrane system has demonstrated considerable performance and leakage concerns, these concerns will not be an issue in the final design when the proven COTS design will be applied.

D. Carbon Formation Reactor Performance Testing Results and Discussion

The CFR was packed with MRS and steel beads and tested to evaluate the performance with feed streams containing only CO and hydrogen. This simple test had two advantages. First, the simple inlet streams most closely mimicked those used in sub-scale testing conducted to obtain critical design parameters. Second, the low complexity of the test provided the most flexibility for test conductors to explore any anomalies or to troubleshoot in real-time.

1. Thermal Performance of CFR

Testing of the CFR began with a thermal evaluation during heating. A total of eight thermocouples were located at the inlet, outlet and within the reactor. Figure 12 and Table 8 provide a visual and descriptive explanation of the relative locations of each thermocouple.
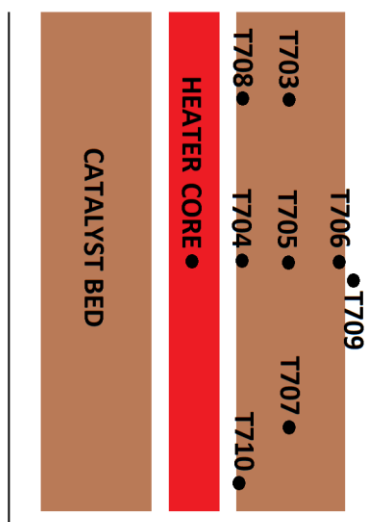

Figure 12. Relative locations of RWGSr thermocouples.

Table 8. Description of thermocouple placement in the Batch Carbon Formation Reactor.

Thermocouple	Description
T703	Located axially within 5" of the top of the reactor and radially at the center of the catalyst bed
T704	Located axially at the midpoint in the reactor and radially 0.15" from the inlet of the catalyst bed
T705	Located axially at the midpoint in the reactor and radially 0.4" from the inlet of the catalyst bed
T706	Located axially at the midpoint in the reactor and radially 0.65" from the inlet of the catalyst bed
T707	Located axially within 5" of the bottom of the reactor and radially at the center of the catalyst bed
T708	Located axially within 5" of the top of the reactor and radially at the exit of the catalyst bed
T709	Located axially within 5" of the bottom of the reactor and radially at the exit of the catalyst bed
T710	Located axially at the exit point of the gas from the heater annulus and radially at the entrance of the catalyst bed

11

The thermal profile of the reactor was first analyzed while packed with MRS. MRS is known to have very low thermal conductivity, so a long heat-up time was expected in order to reach steady state. Thermal modeling during the reactor design phase suggested that insulating the reactor might lead to excessive temperatures near the reactor thermocouple leads. Thus, the reactor was not insulated for this test. Figure 13 shows a plot of the reactor temperatures versus time. As can be seen in the figure, the catalyst bed never reached a temperature greater than 440°C despite the core heater temperature set to 750°C. In an effort to achieve higher temperatures at the inlet to the catalyst bed, a pre-heater was placed on the inlet line to the reactor. Even when preheating the inlet gas to 400°C, no change in temperature was observed at any point in the catalyst bed. Regardless, the test was continued with the performance to provide a baseline for future testing and for future design modifications.

Figure 13. Thermal profile of Batch CFR packed with MRS during heat-up.
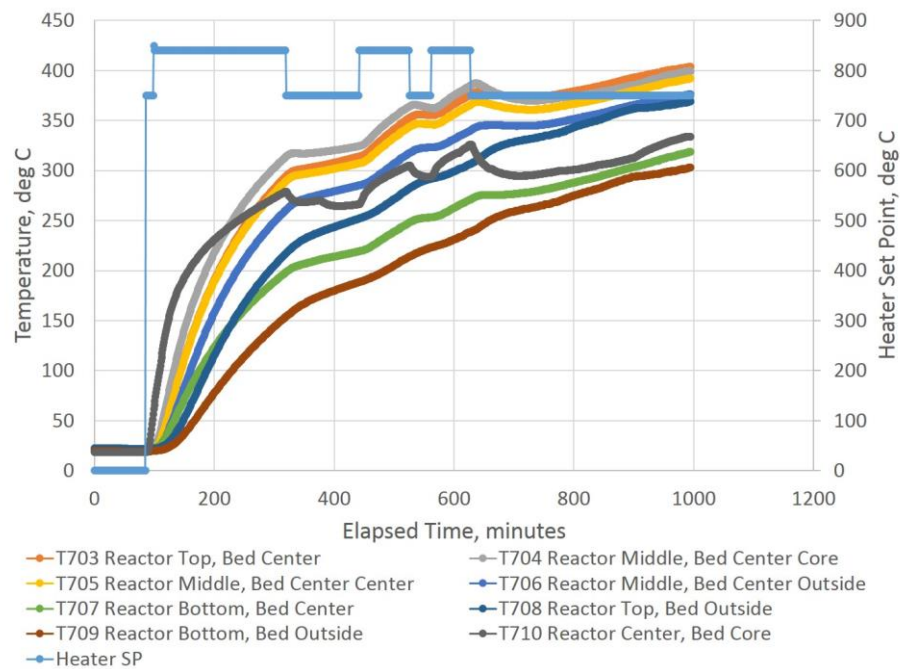
Figure 14. Thermal profile of Batch CFR packed with steel beads during heat-up.

A similar thermal profile was obtained for the reactor when packed with steel beads. A key difference with the steel beads was that the reactor was wrapped with ½" thick nonwoven ceramic insulation (2 layers on the bottom and 4 layers on all other surfaces) in an effort to achieve higher catalyst bed temperatures than were achieved in the MRS test. Data points collected included the same conditions as those run for the MRS catalyst, (*with the important caveat that the core heater was operated at 750˚C, rather than 700˚C*. Figure 14 demonstrates that catalyst bed temperatures were higher, on average, and more uniform for this test than for the MRS catalyst test: about 325-425˚C versus about 115-425˚C. This may be attributed to the differences in thermal properties (conductivity, heat capacity), as well as differences in properties influencing convective heat transfer (porosity, tortuosity) and reaction kinetic rates, between the two catalyst materials, in addition to any improvement in heat retention as a result of the added insulation.
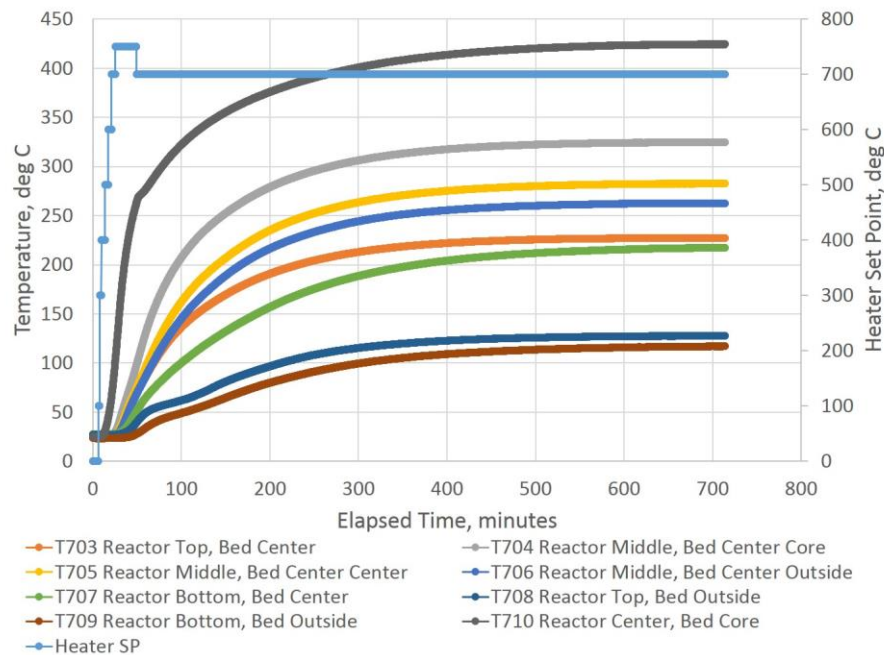
International Conference on Environmental Systems

2. BCFR Performance with MRS

Based on the design, and the assumption that the inlet to the catalyst bed would achieve at least 600°C, the MRS catalyst was predicted to achieve ~75% single-pass conversion of CO at a CO flow rate of 0.195 SLPM with an equimolar ratio of hydrogen. As can be seen in Figure 15, only 20% conversion was achieved. This can be directly attributed to the low temperature at the inlet of the bed and the resulting kinetic limitations of the reactgor. Similarly, for a CO flow rate of 0.385, an even lower conversion was observed. This data suggests that insulating the reactor will be critical with the current design. Additional testing with insulation will be
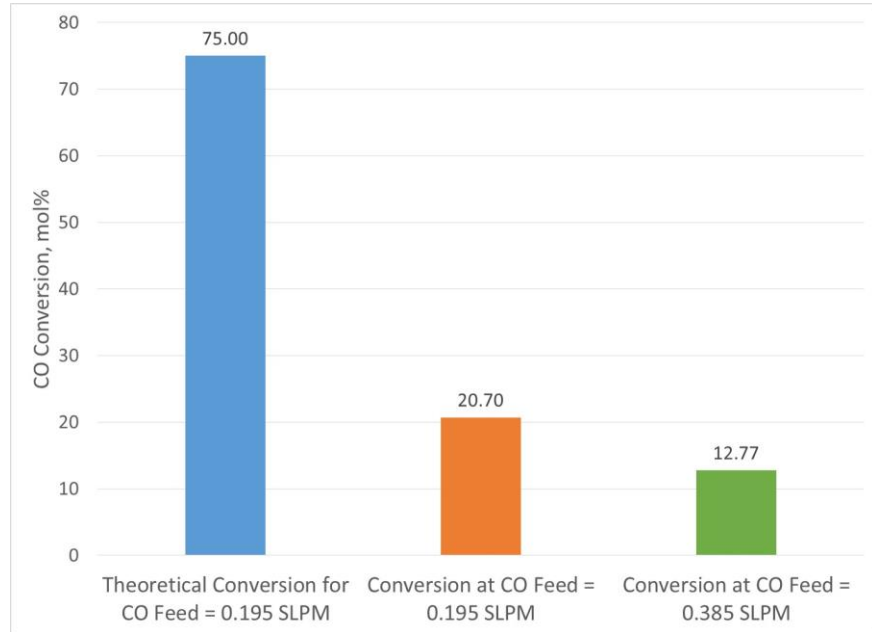

Figure 15. Carbon monoxide conversion in the Batch Carbon Formation Reactor containing Martian Regolith simulant catalyst.

required to fully evaluate the performance of the reactor with the MRS catalyst.

3. BCFR Performance with Steel Beads

Net percentage conversions of carbon monoxide are shown in Figure 16 as a function of the CO feed rate (SLPM). The first nine data points gathered were at 16.0 psia. These data points clearly do not fit the trends demonstrated by all the other data points collected. Because this difference in performance was observed, the data points collected at 16.0 psia and 1.00 H_2:CO ratio were repeated at the end of the test. These data points are labeled as "repeats", while those initially collected at 16.0 psia and 1.00 H_2:CO ratio are labeled as "first round". One additional CO molar feed
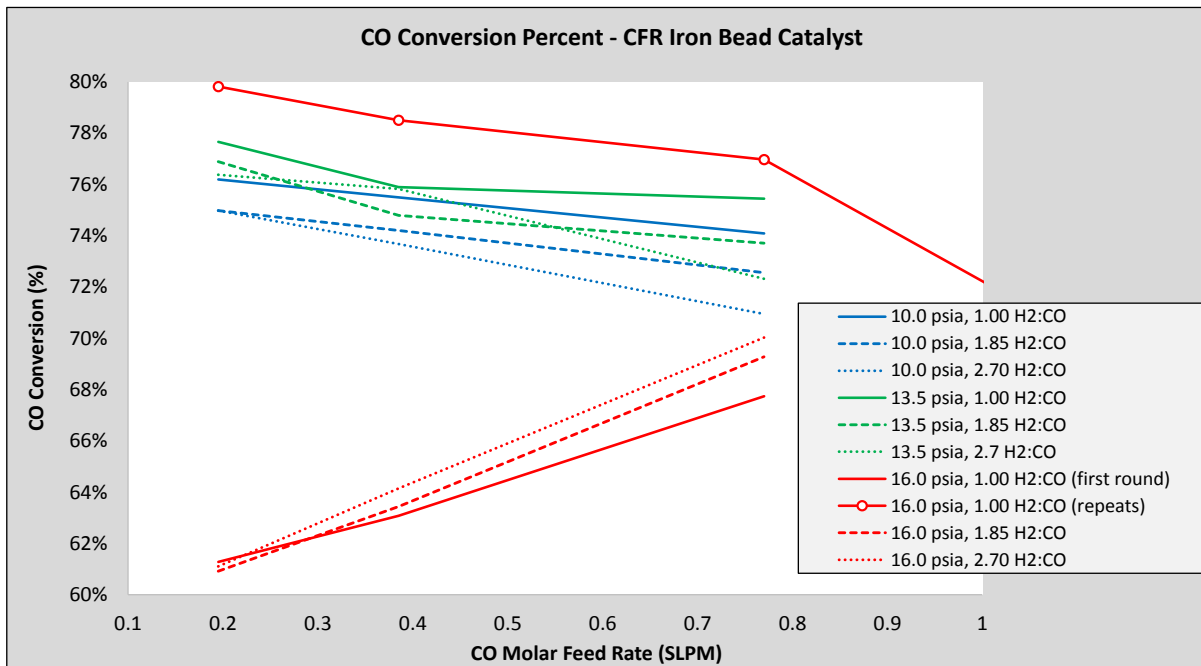

Figure 16. Net CO conversion percentages for the CFR Iron Bead Catalyst Test.

13

International Conference on Environmental Systems

(2.00 SLPM) rate was tested with the "repeats" and is beyond the upper limit of the x-axis in Figure 16. We suspect that the discrepant results of the initial nine data points were caused in part by the lower temperatures in the catalyst bed, which was still increasing in temperature during the first nine data points (779-1436 minutes), and reached a reasonably steady state by the tenth data point (1729 minutes).

Overall, the steel beads performed exceptionally well, demonstrating the predicted performance based on pre-fabrication design despite operating at a considerably lower temperature than intended. A key finding of this data is the considerably higher CO conversion at 0.195 SLPM CO feed with the steel beads as compared to MRS. Whereas MRS achieved only ~20% CO conversion, under similar conditions, the steel beads achieved ~78% CO conversion, despite the similar temperatures in the reactor. This draws a clear comparison with respect to the efficiency of the steel bead catalyst as compared to MRS. Previous testing has demonstrated a specific carbon capacity of ~200g carbon/g iron. If this could be achieved using the steel beads, a total mass of ~10 kg of catalyst would be required to maintain a crew of four on a 5-year mission. While using Martian regolith as a catalyst for a life support system would take advantage of an *in situ* resource and be a nearly inexhaustible life support resource, one must acknowledge the risks of variable iron content, trace contaminants, and the presence of perchlorate in the Martian regolith. Baselining a steel catalyst for an S-Bosch system would increase the mass of required catalyst resupply from Earth (2 kg vs 10 kg), but the comparative mass may be worth the decreased risk.

E. S-Bosch Approach and Advantages of the Architecture

As mentioned previously, the S-Bosch architecture involves several sub-assemblies including an RWGSr, two separation membranes, and a CFR. Under normal operation, this approach provides the optimized operation of the RWGSr and CFR to maximize single-pass conversion of CO_2 and water production, thereby minimizing overall system mass. A second benefit of this approach is in the exceptional robustness provided by the sub-assembly architecture. Single-point failures of primary sub-systems including the separation membranes, the RWGS reactor, and the CFR will not cause a complete shut-down of the system. The only failures that would cause a system shutdown would be from the water separation system (a system already proven reliable in flight), or the vacuum pump (likely an on-orbit replacement unit that could be easily replaced). Three potential failures and responses are provided below.

1. Membrane Failure (shown in Figure 17): Per the architecture, fresh gas "collects" recycled CO_2 and H_2 from the separation membranes before being fed to the RWGS reactor. In the event of membrane failure, the fresh gas feed may be directly fed to the RWGSr. The RWGSr product gas would then be fed directly to the CFR. The CFR product stream would simply be recycled. This
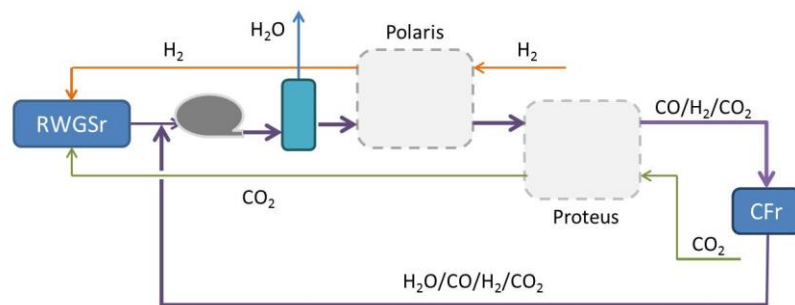

Figure 17. S-Bosch system in the event of membrane failure. *Inlet fresh feed/sweep gas is fed directly to the RWGS reactor. No CO_2 or H_2 recycle to the RWGS leads to a larger recycle stream in the CFR loop.*

would reduce the single-pass efficiency of the CFR, but would not cause the system to shut down. The ultimate result could be a combination of several effects: the flow rate in the CFR recycle stream could increase (requiring additional power consumption by the vacuum pump and heaters), the pressure and temperature in the CFR could increase, and/or the feed rates of H_2 and CO_2 to the system could decrease, but would not cause the system to be shut-down, nor would it reduce the overall system O_2 recovery.

2. RWGS Reactor Failure (shown in Figure 18): If the RWGS reactor should fail, the S-Bosch system simply becomes a traditional Bosch system in which all of the gas feed goes directly to the CFR. Again, the single pass efficiency of the system decreases, the vacuum pump and other components consume additional power to maintain the processing rate, but the system continues to recover O_2 from CO_2 at a large fraction of the nominal rate, or even at the nominal rate.
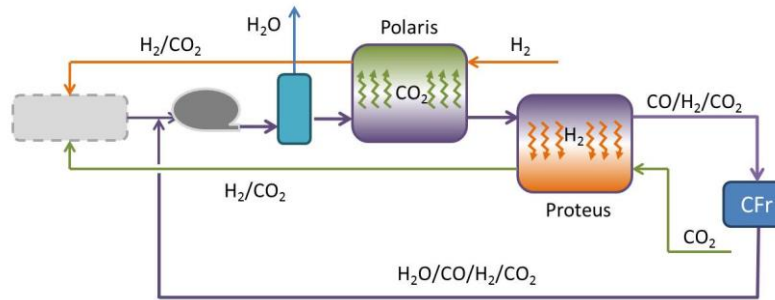

Figure 18. S-Bosch system in the event of RWGS reactor failure. *Inlet fresh feed/sweep gas is fed directly to the CFR loop. No initial RWGS reaction leads to a larger recycle stream in the CFR loop.*

3. CFR Failure (shown in Figure 19): If the CFR should fail, the fresh gas would still collect CO_2 and H_2 from the RWGS product gases when passing through the separation membranes. The remaining product gases would be vented. The fresh feed gas would be fed to the RWGS and reduced. At this time, there are two options. First, the RWGS may be operated nominally and the resulting O_2 recovery will be approximately 40% (similar to the 50% recovery by Sabatier

Figure 19. S-Bosch system in the event of CFR failure. *RWGS reactor product gas is vented after removal of H_2 and CO_2 via the membranes.*

technology). This is because the RWGS reactor has a single-pass conversion of ~50% at 650°C and a portion of the unreacted CO_2 and H_2 are recycled via the separation membranes. As a secondary option, the RWGS operation temperature may be increased to increase the single-pass conversion. This will achieve a theoretical maximum of 50% O_2 recovery.
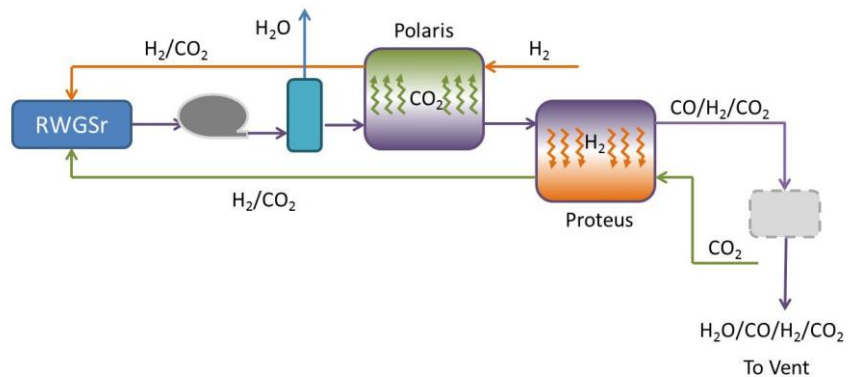
Overall, success of this approach offers a revolutionary and transformational approach to long-duration life support in that maximum oxygen recovery may be achieved with minimal resupply in a highly robust and operationally flexible system.

IV. Conclusions and Future Work

The RWGS reactor demonstrated acceptable performance based on design predictions and anticipated flow rates. The Proteus membrane performed as advertised by the vendor, MTR. The hydrogen selectivity and total permeability is acceptable for an S-Bosch system. The Polaris membrane did not perform as advertised likely due to a combination of a hole in the membrane material and poor sealing of the membrane in the house. However, this is a problem that is irrelevant to the final S-Bosch design due to the COTS approach that will be employed for the final membrane iteration. The CFR did not perform as anticipated due to significant thermal losses that were not anticipated in pre-design thermal models. This reduction in the performance was most evident with the Martian Regolith Simulant as a catalyst. Future testing with MRS will involve insulating the reactor in an attempt to increase reactor temperatures. Testing with the steel beads showed impressive performance despite the temperatures well below those originally intended. Future work will involve testing of these catalysts in a continuous CFR. Finally, integrated testing of all pieces of the S-Bosch system will be completed to achieve a system level technology readiness level of 5.

References

[1]Hurlbert, K., Badgidian, B., Carroll, C., Jeevarajan, A., Kliss, M., Singh, B.; "Human Health, Life Support, and Habitation Systems, Technology Area 06," *NASA Space Technology Roadmaps*, http://www.nasa.gov/offices/oct/home/roadmaps, accessed March 10, 2014.

[2]Atwater, J. E., Wheeler, R. R., Jr., Hadley, N. M., Dahl, R. W., Carrasquillo, R. L., "Development and Testing of a Prototype Microwave Plasma Reactor for Hydrogen Recovery from Sabatier Waste Methane," *39th International Conference on Environmental Systems,* SAE International, SAE 2009-01-2467, Savannah, Georgia, 2009.

[3]Abney, M.B., Miller, L.A., Williams, T., "Sabatier Reactor System Integration with Microwave Plasma Methane Pyrolysis Post-Processor for Closed-Loop Hydrogen Recovery," *40th International Conference on Environmental Systems*, AIAA-2010-6474, Barcelona, Spain, 2010.

[4]Mansell, J. M., Abney, M. B., and Miller, L. A., "Influence of Oxygenated Compounds on Reaction Products in a Microwave Plasma Methane Pyrolysis Assembly for Post-Processing of Sabatier Methane," AIAA Paper No. 2011-5035, presented at the 41st International Conference on Environmental Systems, Portland, 2011.

[5]Wheeler, R.R. Jr., Hadley, N.M., Dahl, R.W., Abney, M.B., Greenwood, Z., Miller, L., Medlen, A., "Advanced PPA Reactor and Process Development," AIAA Paper No. 2012-3553-145, presented at the 42nd International Conference on Environmental Systems, San Diego, CA, 2012.

[6] Abney, M. B., Miller, L. A., and Barton, K., Evaluation of Sorbents for Acetylene Separation in Atmosphere Revitalization Loop Closure, AIAA Paper No. 2011-5057, presented at the 41st International Conference on Environmental Systems, Portland, 2011.

[7]Abney, M.B., Mansell, J.M, *et al.,* "Series-Bosch Technology For Oxygen Recovery During Lunar or Martian Surface Missions," *44th Annual Conference on Environmental Systems,* Pheonix, AZ, July 2014.

[8]Abney, M.B., Mansell, J.M., "The Bosch Process - Performance of a Developmental Reactor and Experimental Evaluation of Alternative Catalysts," *40th Annual Conference on Environmental Systems,* AIAA Technical Paper, AIAA-2010-6272, Barcelona, Spain, July 11-15, 2010.

[9]Abney, M.B., Mansell, J.M., "Evaluation of Bosch-Based Systems Using Non-Traditional Catalysts at Reduced Temperatures," *AIAA International Conference on Environmental Systems*, AIAA-2011-5059, Portland, OR, July 17-21, 2011.

[10]Abney, M. B., Evans, C., Mansell, M., and Swickrath, M., "Series Bosch System Development," *AIAA International Conference on Environmental Systems*, AIAA 2012-3554, AIAA, San Diego, CA, 2012.

[11]Abney, M. B., Mansell, J. M., Stanley, C., Edmunson, J., DuMez, S. J., Chen, K., "Ongoing Development of a Series Bosch Reactor System," *AIAA International Conference on Environmental Systems*, AIAA 2013-3512, AIAA, Vale, CO, 2013.

[12] Norcross, J., Norsk, Pl, Law, J., Arias, D., Conkin, J., Perchonok, M., Menon, A., Huff, J., Fogarty, J., Wessel, J.H., Whitmire, S., "Effects of the 8 psia / 32% O2 Atmosphere on the Human in the Spaceflight Environment", NASA TM-2013-217377, 2013.